noxin, a Novel Stress-Induced Gene Involved in Cell Cycle and Apoptosis[▽]

Naoki Nakaya,[1]† Jill Hemish,[1,2]† Peter Krasnov,[1] Sang-Yong Kim,[1] Yuri Stasiv,[1] Tatyana Michurina,[1]
Daniel Herman,[1] Michail S. Davidoff,[3] Ralf Middendorff,[4] and Grigori Enikolopov[1]*

*Cold Spring Harbor Laboratory, Cold Spring Harbor, New York 11724[1]; Graduate Program in Genetics, SUNY at Stony Brook,
Stony Brook, New York 11794[2]; Institute of Anatomy, University of Hamburg, 20246 Hamburg, Germany[3]; and
Institute of Anatomy and Cell Biology, Justus Liebig University, 35385 Giessen, Germany[4]*

We describe a novel stress-induced gene, noxin, and a knockout mouse line with an inactivated noxin gene. The noxin gene does not have sequelogs in the genome and encodes a highly serine-rich protein with predicted phosphorylation sites for ATM, Akt, and DNA-dependent protein kinase kinases; nuclear localization signals; and a Zn finger domain. noxin mRNA and protein levels are under tight control by the cell cycle. noxin, identified as a nitric oxide-inducible gene, is strongly induced by a wide range of stress signals: γ- and UV irradiation, hydrogen peroxide, adriamycin, and cytokines. This induction is dependent on p53. Noxin accumulates in the nucleus in response to stress and, when ectopically expressed, Noxin arrests the cell cycle at G_1; although it also induces p53, the cell cycle arrest function of Noxin is independent of p53 activity. noxin knockout mice are viable and fertile; however, they have an enlarged heart, several altered hematopoietic parameters, and a decreased number of spermatids. Importantly, loss or downregulation of Noxin leads to increased cell death. Our results suggest that Noxin may be a component of the cell defense system: it is activated by various stress stimuli, helps cells to withdraw from cycling, and opposes apoptosis.

Cells respond to oxidative and genotoxic stress by withdrawing from the cell cycle, repairing the damaged regions of DNA, repairing or destroying affected proteins, altering growth characteristics, and seeking to inactivate the stressor. Alternatively, if the stress-induced damage is too extensive, cells may be eliminated by apoptosis. Various stressors (e.g., ionizing radiation, UV radiation, reactive oxygen and nitrogen species, and alkylating chemicals) act differently and cause distinct types of damage to the cell; at the same time, these dissimilar insults activate shared sets of molecules and pathways aimed at minimizing the damage and repairing the affected cell components (1, 11, 12, 16). The cellular defense mechanisms include immediate responses (e.g., posttranslational modifications of the tumor suppressor protein p53, leading to its accumulation in the cells), as well as more extended responses (e.g., transcriptional activation of sets of crucial genes whose products help the cells to complete the repair process or to communicate the stress and repair signals to the surrounding cells). Together, this coordinated set of protein modification and gene activation events helps ensure that the damage to cells is minimized and that cells restore their prestress status (e.g., return to cycling).

Nitric oxide (NO) is a versatile signaling molecule that is involved in both physiologic (e.g., vasorelaxation and neurotransmission) and pathological (e.g., inflammation and cell death) processes in the organism (3, 15, 19). When produced at high levels (e.g., by the high-output inducible NOS isoform), it can induce cell damage and subsequent apoptosis (4, 17). At lower levels, NO can act as an antiproliferative agent in vitro

and in vivo, contributing to cell cycle arrest during cell differentiation or inflammation. When acting upon the cell cycle machinery, NO affects multiple pathways and can contribute to cell cycle arrest through several independent mechanisms (5, 8–10, 19, 20, 22). Several major regulators of the cell cycle and stress response, e.g., cyclin-dependent kinase 2 (cdk2), cdk inhibitor p21/WAF, cyclin D1, PCNA, ribonucleotide reductase, mdm2, p53, and ataxia telangectasia mutated kinase (ATM) are involved in the cellular response to NO (2, 14, 18, 24, 25). Given the extent of NO involvement in cell physiology, it is likely that specific additional components mediate the response to NO in particular contexts. At the same time, it is conceivable that responses to NO engage mechanisms that are employed by cells in responding to other stressful stimuli.

While searching for NO-inducible genes, we identified a new gene that was strongly induced by different NO donors. We found that this gene, noxin, was also strongly induced by a range of other stress stimuli. Here, we describe noxin as a novel component of the stress response system and describe a line of knockout mice in which the noxin gene has been inactivated. We show that Noxin expression is regulated throughout the cell cycle, that its expression is strongly induced by stress, that it can effectively induce arrest of cells in G_1 phase, and that its loss leads to increased apoptosis. Our results suggest that noxin may be an important component of the repair machinery of the stressed cell.

MATERIALS AND METHODS

Cell culture and reagents. NIH 3T3 fibroblasts were maintained at 37°C in an atmosphere of 5% CO_2 in Dulbecco modified Eagle's medium (DMEM) with 10% calf serum. Mouse embryonic fibroblasts (MEFs) were isolated from embryonic day 13 to 14 mouse embryos, treated with trypsin, and cultured in DMEM with 10% fetal calf serum. S-Nitroso-N-acetyl-D,L-penicillamine (SNAP), 1-hydroxy-2-oxo-3-(N-ethyl-2-aminoethyl)-3-ethyl-1-triazene (NOC12), and DETA NONOate (NOC18) were purchased from Calbiochem and used at a concentration of 250 μM. Adriamycin (Sigma) and hydrogen peroxide (Sigma)

---

* Corresponding author. Mailing address: Cold Spring Harbor Laboratory, 1 Bungtown Road, Cold Spring Harbor, NY 11724. Phone: (516) 367-8316. Fax: (516) 367-6805. E-mail: enik@cshl.edu.
† N. Nakaya and J. Hemish contributed equally to this study.
▽ Published ahead of print on 21 May 2007.

were added to the cultures at concentrations of 0.1 μg/ml and 5 μM, respectively. γ-irradiation was performed at 10 Gy to induce *noxin* mRNA using a γ-irradiator (Atomic Energy of Canada; Mark I cesium-137 irradiator). UV irradiation (120 J/m^2) was performed by placing cell culture plates in the transilluminator (Fotodyne, Inc.). The following cytokines were used: tumor necrosis factor alpha (TNF-α) (10 ng/ml; R&D Systems), gamma interferon (IFN-γ) (200 U/ml; Calbiochem), and interleukin-1β (IL-1β) (200 pg/ml; R&D Systems).

Cell cycle synchronization. NIH 3T3 cells and MEFs were cultured for 24 h in DMEM containing 0.5% and 0.1% calf serum, respectively, to synchronize them in G_0 phase. The cells were stimulated to reenter the cell cycle by replacing the medium with DMEM (10% calf serum). For synchronization in the S and G_2/M phases, cells were treated for 20 h with aphidicolin (6 μM) or nocodazole (100 ng/ml), respectively.

Plasmid construction. cDNA encoding the entire Noxin polypeptide was excised from IMAGE clone AI157360 (Research Genetics) with XhoI and subcloned into pcDNA3 (Invitrogen). The 5′-end XhoI-HindIII *noxin* cDNA fragment was amplified by PCR using primers with a two-FLAG-tag sequence and used to replace the original Noxin sequences to generate the pFLAG-noxin expression plasmid. Plasmids expressing p53, p53dn (a dominant-negative form of p53), and p21/WAF were gifts from S. Lowe (Cold Spring Harbor Laboratory). pEGFP-N1, pCFP-nuc, and pYFP-actin were purchased from Clontech.

***noxin* shRNA constructs.** Plasmids expressing six different *noxin* short hairpin RNAs (shRNAs) (HPA to HPF) under the control of the human U6 promoter were generated as described previously (21). U6 promoter cassette DNA was amplified using a 5′ primer corresponding to the SP6 site at the 5′ end of the U6 promoter cassette and a long 3′ primer complementary to the 3′ end of the promoter and containing sequences for the *noxin* shRNA and a polymerase III termination site. The PCR fragments obtained were subcloned into pENTR-TOPO-D vector (Invitrogen) and then transferred into pMSCV-puro vector by a clonase (Invitrogen) reaction.

Total-RNA extraction and poly(A)$^+$ RNA isolation. Cells cultured in 10-cm plates were lysed with 2 ml of TRIzol (Invitrogen), and total RNA was isolated according to the manufacturer's protocol and then resuspended in 10 mM Tris-HCl, 1 mM EDTA, pH 7.4, buffer at a final concentration of 2 μg/μl. poly(A)$^+$ RNA was isolated using the FastTrack 2.0 kit (Invitrogen) according to the manufacturer's instructions.

cDNA microarray analysis. Total RNA was isolated from untreated cells and cells treated with NO donors: SNAP, NOC12, and NOC18. NO-induced gene expression changes were determined by cDNA microarray analysis as described previously (13). Briefly, poly(A)$^+$ RNA samples were labeled with Cy5 or Cy3 fluorescent dye and hybridized to custom printed slide arrays produced by the Cold Spring Harbor Laboratory Genome Center. After being washed, the microarray slides were scanned using a GenePix scanner and software (version 3.0; Axon Instruments, Inc.).

Real-time quantitative reverse transcription-PCR (Q-PCR). Total RNA (2 μg) was converted into cDNA by Taqman Multiscribe reverse transcriptase (125 U; Applied Biosystems) using random hexamer primers. The cDNA was diluted, mixed with 2× SYBR Green PCR Master Mix (Applied Biosystems) and 0.3 μM both forward and reverse primers, and amplified using the ABI PRISM 7700 Sequence Detection System (Applied Biosystems). The following primers (Sigma Genosys) for *noxin* and β-actin were designed using Primer Express software (Applied Biosystems), assuming a melting temperature of 58 to 60°C and an amplicon size of 70 to 150 bp: 5′-TTTCTACCGGATACTTGCTCATCA-3′ (noxin-FW), 5′-GTTGCAAGACCCCACTAGTCCT-3′ (noxin-RV), 5′-CGTG AAAAGATGACCCAGATCA-3′ (β-actin-FW), and 5′-CACAGCCTGGATG GCTACGTA-3′ (β-actin-RV).

The PCR conditions for the thermal cycler were as follows: denaturation (1 cycle at 95°C for 10 min) and amplification (40 cycles at 95°C for 15 s and 60°C for 1 min). During amplification, the fluorescence of each sample in the plate was detected in real time and an amplification curve was drawn with Sequence Detection System Software (Applied Biosystems) to get the threshold cycle, the cycle number at which the curve started to rise over the background noise. The data from *noxin* amplifications were normalized using the threshold cycle value from the β-actin set for each sample, and the difference between the amounts of *noxin* RNA in untreated and in stress-exposed cells was calculated.

Northern blot analysis. Total RNA (10 μg) was separated by denaturing formaldehyde-agarose gel electrophoresis and transferred onto a nylon membrane (Hybond-N$^+$; Amersham). The membrane was prehybridized with hybridization buffer (0.05 M sodium phosphate buffer, 5× SSC [1× SSC is 0.15 M NaCl plus 0.015 M sodium citrate], 4× Denhardt's solution, 1% sodium dodecyl sulfate [SDS], 50% formamide, 0.1 mg/ml salmon sperm DNA, and 0.2 mg/ml yeast tRNA) for 6 h at 42°C and hybridized with the same buffer containing 100,000 cpm/ml [α-^{32}P]dCTP-labeled *noxin* cDNA probe amplified by PCR from

pFLAG-noxin. Following hybridization for 20 h at 42°C, the membrane was washed twice with 2× SSC for 5 min each time at room temperature, twice with 0.2× SSC for 5 min each time at 65°C, and twice with 1× SSC with 3% glycerol for 5 min each time at room temperature. The membrane was exposed for 3 days at −70°C to X-OMAT X-ray film (Kodak).

5′-RACE. 5′ rapid amplification of cDNA ends (RACE) was performed using the FirstChoice RLM-RACE kit (Ambion) according to the manufacturer's instructions. Poly(A)$^+$ RNA isolated from adult mouse testes was reverse transcribed into cDNA. A specially designed adaptor sequence provided in the RLM-RACE kit was ligated to the ends of the cDNA, and the adaptor primer served as the forward primer. An antisense gene-specific primer (5′-GAAGCA CCTTTGACATGATGGA-3′) derived from nucleotides 270 to 291 in the *noxin* cDNA and an antisense gene-specific primer (5′-TGGCCCTTCTTGGCATAA TG-3′) derived from nucleotides 125 to 144 served as the outer and nested primers, respectively. The PCR products were cloned into pCRII-TOPO vector (Invitrogen) and sequenced.

Western blot analysis. Cells or tissues were homogenized in lysis buffer (10 mM Tris-HCl, pH 7.5, 1 mM EDTA, 400 mM NaCl, 0.5% NP-40, 5 mM NaF, 0.5 mM sodium orthovanadate, 10% glycerol, 1 mM dithiothreitol, 1 mM phenylmethylsulfonyl fluoride, 1 μg/ml aprotinin, 1 μg/ml leupeptin, and 1 μg/ml pepstatin) for 20 min on ice. Following centrifugation, the soluble fraction was collected and the protein concentration was determined using a bicinchoninic acid assay kit (Pierce). Fifty micrograms of total protein was separated on an 8% SDS-polyacrylamide gel electrophoresis gel and transferred to an Immobilon-P membrane (Millipore Corporation) by semidry blotting. The membranes were incubated with anti-FLAG antibody (1:1,000; Sigma) or anti-Noxin antibody (1:1,000), followed by anti-mouse immunoglobulin G (IgG) or anti-rabbit IgG antibody conjugated to horseradish peroxidase (HRP) (1:10,000; Amersham). The HRP signal was detected using a chemiluminescence detection kit (SuperSignal Femto Dura Extended Duration Substrate; Pierce) and Hyperfim X-ray film (Amersham Biosciences).

Immunocytochemistry. Cells grown on coverslips coated with collagen and poly-L-lysine were fixed with 4% methanol-free formaldehyde in phosphate-buffered saline (PBS) for 20 min on ice. After permeabilization with 0.1% Triton X-100 in PBS for 10 min on ice, the cells were incubated with primary and secondary antibodies in PBS (containing 0.05% Tween 20 and 1% bovine serum albumin [BSA]) each for 1 h at room temperature. The primary antibodies used in these experiments were anti-FLAG (1:500; Sigma), anti-p53 (1:1,000; Novocastra), and fluorescein isothiocyanate (FITC)-conjugated anti-8-bromodeoxyuridine (BrdU) antibody (1:500; Pharmingen). The secondary antibodies were ALEXA Fluor 488-conjugated goat anti-mouse IgG (1:500; Molecular Probes) and ALEXA Fluor 546-conjugated goat anti-rabbit IgG (1:500; Molecular Probes). Cell nuclei were counterstained with Hoechst 33342 (Molecular Probes), and the coverslips were mounted with Gel/Mount medium (Biomega). Fluorescence signals were analyzed under a fluorescence microscope (Zeiss Axiophot) equipped with Plan-Neofluar objectives (40 to 100×) and a charge-coupled device camera. Data were analyzed with Photoshop software (version 6; Adobe).

In situ hybridization. Adult mouse (C57BL/6) tissues were directly frozen in OCT compound (Tissue-Tek), sectioned by cryostat (10-μm thickness), and mounted on glass slides (ProbeOn Plus; Fisher). The *noxin* cDNA PCR fragment was subcloned into pCRII-TOPO. Digoxigenin (DIG)-labeled *noxin* RNA probes were transcribed from SacI-linearized constructs in vitro using T7 RNA polymerase (DIG RNA Labeling kit; Boehringer Mannheim) according to the manufacturer's instructions. Hybridized RNA was detected using alkaline phosphatase-conjugated anti-DIG according to the procedure described previously (6).

Flow cytometry analysis and cell cycle determination. BrdU-labeled (10 μM) cells collected from plates by trypsin digestion were suspended in saline and fixed with 70% ethanol. After being washed with PBS with 0.05% BSA, 1×10^6 cells were incubated with FITC-conjugated anti-BrdU antibody (Pharmingen; 1:500) for 1 h, suspended in PBS-BSA with 5 μg/ml propidium iodide (PI) and 20 μg/ml RNase A, and incubated further for 30 min at room temperature. For bivariate cell cycle analysis, cells were analyzed using an LSRII flow cytometer (Perkin-Elmer). For the detection of p53 by cytometric analysis, pFLAG-noxin- or pEGFP-transfected cells were fixed with 4% paraformaldehyde, permeabilized with saponin, and stained with primary antibodies (CM5 anti-p53 polyclonal antibody and M1 anti-FLAG monoclonal antibody, both from Sigma) and then with secondary antibodies (phycoerythrin [PE]-conjugated goat anti-rabbit IgG and FITC-labeled goat anti-mouse IgG). Cells were analyzed for PE, FITC, and green fluorescent protein (GFP) fluorescence by flow cytometry.

***noxin* knockout mice.** The bacterial artificial chromosome (BAC) containing the entire *noxin* gene was obtained by screening the BAC library with the *noxin*

cDNA clone. The resulting BAC clone was digested with EcoRI and HindIII to isolate the left and right arms of the targeting construct, respectively. After digestion and gel separation, 2-kb and 3-kb fragments were subcloned to flank both sides of the neomycin resistance gene in the pPNT vector, generating the *noxin* targeting vector pPNT-noxin. Cultured embryonic stem cells were transfected with pPNT-noxin, and neomycin-resistant clones were selected for by treatment with G418. Four hundred neomycin-resistant clones were screened by nested PCR and further by genomic Southern blots. Two of the seven positive embryonic stem cell clones were injected into mouse blastocysts, and mice were generated using standard techniques. The mice were genotyped by PCR using primer sets specific for the wild-type and knockout alleles.

Detection of endogenous Noxin protein. Anti-Noxin antiserum was raised by immunizing a rabbit with a peptide sequence located at the C-terminal region (870 to 886) of Noxin (RKCLDLHYSPDPKELPR). For immunohistochemistry, mice were perfused transcardially with PBS and then with 4% paraformaldehyde in PBS at 4°C. Dissected testes were postfixed for 4 h and cryoprotected in 30% sucrose overnight at 4°C. Sections were cut on a cryostat (10-µm thickness) and collected on coated slides (ProbeOn Plus; Fisher). The slides were gradually dehydrated, air dried, and stored at −20°C. Following rehydration, the slides underwent an antigen retrieval step: 10 min of incubation at 95 to 100°C in 0.01 M sodium citrate (pH 6.0), cooling to room temperature, and rinsing with distilled water. The slides were then incubated in 0.3% hydrogen peroxide to inactivate endogenous peroxidases, washed in PBS containing 0.1% Triton X-100 (PBS-T), and blocked at room temperature for 1 h in 3% normal goat serum in PBS-T. The slides were incubated overnight at 4°C with primary antibody (anti-Noxin antibody [1:500]) diluted in PBS-T with 1% goat serum. After being washed with PBS-T, the slides were incubated with a biotinylated goat anti-rabbit secondary antibody (1:200; Vector Laboratories) for 2 h, followed by further washing and incubation in HRP-conjugated avidin-biotin complex (Vector ABC Elite) for 1.5 h before being stained with 3,3′-diaminobenzidine and hydrogen peroxide. All slides were counterstained with hematoxylin, and coverslips were mounted with Permount (Fisher).

Analysis of testis parameters. Immediately after euthanization of adult mice ($n = 6$ for wild-type and $n = 7$ for *noxin*$^{-/-}$ mice), the testes were removed, fixed with 2% glutaraldehyde, and embedded in Epon. Semithin sections (1 µm) were cut on a microtome (Reichert Ultrcut E; Leica, Nussloch, Germany) and stained with toluidine blue-pyronine. For analyzing potential differences in spermatogenesis between wild-type and knockout mice, cross sections of seminiferous tubules displaying the same stages of spermatogenesis were analyzed. We selected intact tubular cross sections of stage VI of spermatogenesis ($n = 93$ for wild-type and $n = 77$ for *noxin*$^{-/-}$ mice) and measured the tubular diameter, which correlates with strong disturbances of spermatogenesis. We also counted the spermatocytes I and round spermatids visible in these tubules. The data are presented as means ± standard errors of the mean of all seminiferous tubules analyzed. Statistical analysis was performed using SPSS Base 12.0 (SPSS Software, Munich, Germany). Differences among experimental groups were analyzed with Mann-Whitney test as installed in SPSS Base, with a P value of ≤0.05 considered significant and a P value of ≤0.01 highly significant.

Cell cycle analysis of MEFs. MEFs isolated from wild-type or *noxin*$^{-/-}$ mice were incubated in low-serum medium (0.5% fetal bovine serum) for 24 h to stop the cell cycle. The medium was then replaced with 10% fetal bovine serum, and SNAP and BrdU were added to the medium. At the end of the incubation, BrdU-labeled cells were stained with FITC-conjugated anti-BrdU antibody and analyzed by flow cytometry.

Detection of apoptotic cells. To detect apoptosis, MEFs isolated from wild-type or *noxin*$^{-/-}$ mice were grown on coverslips coated with collagen and poly-L-lysine, washed with PBS, and processed for the terminal deoxynucleotidyl-transferase-mediated dUTP–fluorescein nick end labeling (TUNEL) assay according to instructions in the ApoAlert DNA Fragmentation Assay Kit (BD Biosciences). TUNEL-positive cells were quantified by microscopy. Wild-type and *noxin*$^{-/-}$ MEFs were also grown in culture, washed with PBS, and stained with a FITC-conjugated annexin V antibody (Molecular Probes) and PI according to the manufacturer's instructions. The percentage of annexin V-positive cells was determined by flow cytometry.

Nucleotide sequence accession number. The *noxin* gene sequence was submitted to GenBank under accession no. DQ400346.

RESULTS

Molecular cloning of *noxin*. We recently determined the temporal order of gene activation induced by NO in mammalian cells (13). Among the genes whose expression was affected

most strongly by three unrelated chemical donors of NO (SNAP, NOC12, and NOC18) (Fig. 1A) was a previously uncharacterized mouse expressed sequence tag (EST) (IMAGE524571 in the I.M.A.G.E. consortium database). This EST sequence was used for further searches, and a larger cDNA clone (GeneID, 74041), which contained the entire coding region of the gene, was identified in the NCBI database. 5′-RACE analysis confirmed that this 3,384-bp-long cDNA contained the 5′ end of the mRNA (with a stop codon preceding the open reading frame) and coded for a protein of 898 amino acids (Fig. 1B), with a predicted molecular mass of 100 kDa and an isoelectric point of 7.23. We raised a polyclonal antibody against a peptide from a C-terminal region of the deduced protein and demonstrated that upon transfection into cultured cells, the cloned cDNA generated a protein with electrophoretic mobility corresponding to that of the endogenous protein (Fig. 2D, f; also see Fig. 4C and 5C and D). We named this gene *noxin* (for *n*itric *ox*ide-*in*ducible). The *noxin* gene is located on mouse chromosome 7 and is conserved (70% similarity at the DNA level) in the rat and human genomes (located on rat chromosome 1 and human chromosome 11) (Fig. 1B). The gene seems to be unique in the rodent and human genomes and does not have obvious closely related sequelogs. An unusual feature of the deduced Noxin protein sequence is that it is very rich in serines (134 serine residues), suggesting phosphorylation of these residues as a possible modification. Indeed, in the extracts of both the animal tissue and cultured NIH 3T3 cells after transfection with the *noxin* cDNA, two distinct bands were apparent on the SDS-polyacrylamide gel (Fig. 2D, f; also see Fig. 4C and 5C and D), and the intensity of the upper band was markedly reduced upon phosphatase treatment (data not shown).

A search for possible phosphorylation sites in Noxin produced consensus sites for modifications by DNA-dependent protein kinase (DNA-PK), ATM, and Akt (Fig. 1C), suggesting that Noxin may be modified by these kinases in response to stress. Noxin also carries two predicted nuclear localization domains near the N and C termini and a part of the C3HC4-type zinc finger domain in the N-terminal region.

Expression of Noxin. Northern blot analysis of RNAs from different mouse tissues showed that Noxin is strongly expressed in the testis and also in the spleen and heart (Fig. 2A). Q-PCR confirmed these data and showed that Noxin expression can also be detected in the bone marrow, brain, lung, liver, and kidney (Fig. 2B).

Strong expression of Noxin in the testis was confirmed and further analyzed by in situ hybridization, immunocytochemistry, and Western blot analysis (Fig. 2). Differentiating male germ cells in the seminiferous epithelium of the testis are spatially and temporally arranged in a distinct pattern that enables their identification: the spermatogonia are localized along the basement membrane at the periphery of the tubules, whereas the primary spermatocytes are localized in the middle layers of the tubules and the spermatids are found close to the lumen (Fig. 2C); furthermore, the distinct morphology of spermatocytes allows their discrimination among the other cell types in the tubules.

Hybridization with the antisense strand of *noxin* cDNA showed that the signal is largely limited to primary spermatocytes, with the sense probe producing no signal (Fig. 2C). This
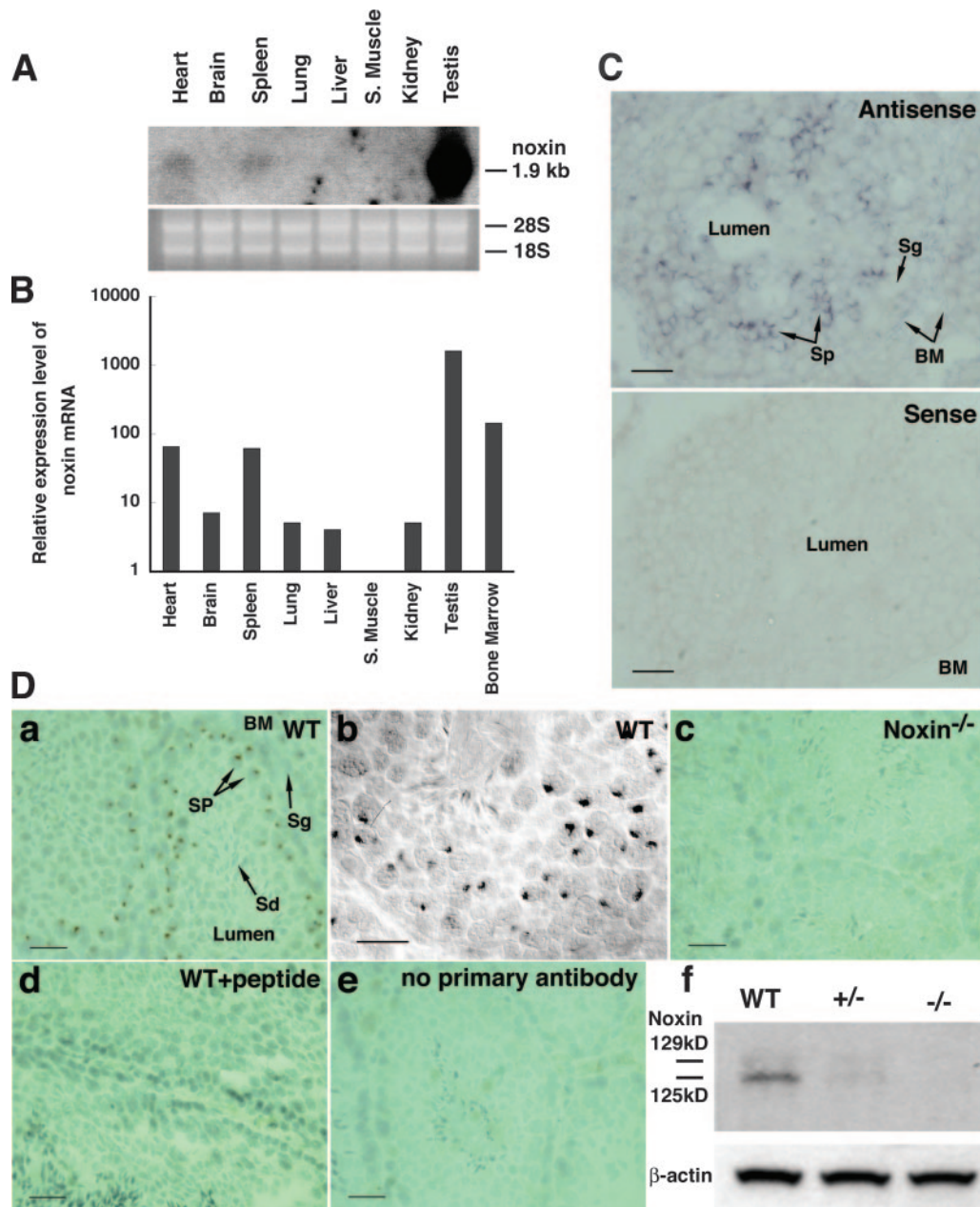
FIG. 1. Cloning of the *noxin* gene. (A) *noxin* is induced by NO donors. Images from microarray analysis showing up-regulation of two distinct genes in a section of the array. NIH 3T3 cells were treated with three different donors of NO (SNAP, NOC12, and NOC18). cDNA probes prepared using RNAs from NO donor-treated and untreated cells were labeled with fluorescent dyes (Cy3 and Cy5, with color reversal) and hybridized to custom cDNA microarray slides. One EST gene, IMAGE524571 (*noxin*), was strongly induced by all three donors; *mdm2* is shown as another example of a strongly induced gene. (B) Deduced amino acid sequence of Noxin. Cloned cDNA of 3,384 bp was sequenced, and the 898-amino-acid-coding region was deduced. Noxin contains a zinc-finger-like domain (light blue) in the N-terminal region; DNA-PK, ATM, and Akt phosphorylation consensus sequences (pink); and two potential nuclear localization signals (red italics). The light-purple letters represent an overlap of the ATM and Akt consensus sequences. Corresponding human and rat partial protein sequences were generated using EST and genome databases. The asterisks denote identical amino acids. (C) Schematic arrangement of protein motifs (represented by the same colors as in panel B) in the Noxin polypeptide.

FIG. 2. Distribution of *noxin* mRNA and protein in adult mouse tissues. (A and B) Total RNA was extracted from different adult mouse tissues and analyzed for *noxin* mRNA by Northern hybridization (A) and Q-PCR (B). The Q-PCR data represent relative amounts of *noxin* mRNA compared to its levels in the skeletal muscle. Testis, bone marrow, spleen, and heart are enriched in *noxin* mRNA. (C) The expression pattern in adult mouse testes visualized by in situ hybridization using a DIG-labeled antisense *noxin* RNA probe (top) and a sense RNA probe (bottom). *noxin* mRNA is mainly expressed in primary spermatocytes. Scale bars, 25 μm. (D) Anti-Noxin antibody reveals immunoreactive structures in or adjacent to the cell nuclei in primary spermatocytes (a). Nomarski images confirm that Noxin protein is localized predominantly in the primary spermatocytes (b). Testes from a *noxin*$^{-/-}$ mouse did not show Noxin signals (c). The staining was eliminated by the addition of the antigen peptide to the primary antibody solution (d) or after staining without the primary antibody (e). Western blot analysis showed that Noxin protein is expressed in the testes of the *noxin*$^{+/+}$ but not of *noxin*$^{-/-}$ animals; its expression is reduced in the *noxin*$^{+/-}$ heterozygotes (f). In images a and b, arrows and labels identify specific tissues and germ cell types: BM, basement membrane; Sg, spermatogonia; Sp, primary spermatocyte; Sd, spermatid. WT, wild type. Scale bar, 25 μm.

was further confirmed by immunocytochemistry, using a polyclonal antibody to Noxin (Fig. 2D). Noxin protein is highly expressed in the primary spermatocytes and, to a lesser extent, in the round spermatids (Fig. 2D, a). This staining is highly specific, as the signal is absent in each of the following: in testes

from *noxin* knockout animals (Fig. 2D, c); in the presence of the peptide used to raise the antibody, added as a competitor (Fig. 2D, d); or in the absence of the primary antibody (Fig. 2D, e). Antibody staining, particularly when visualized using Nomarski imaging (Fig. 2D, b), demonstrates that in primary
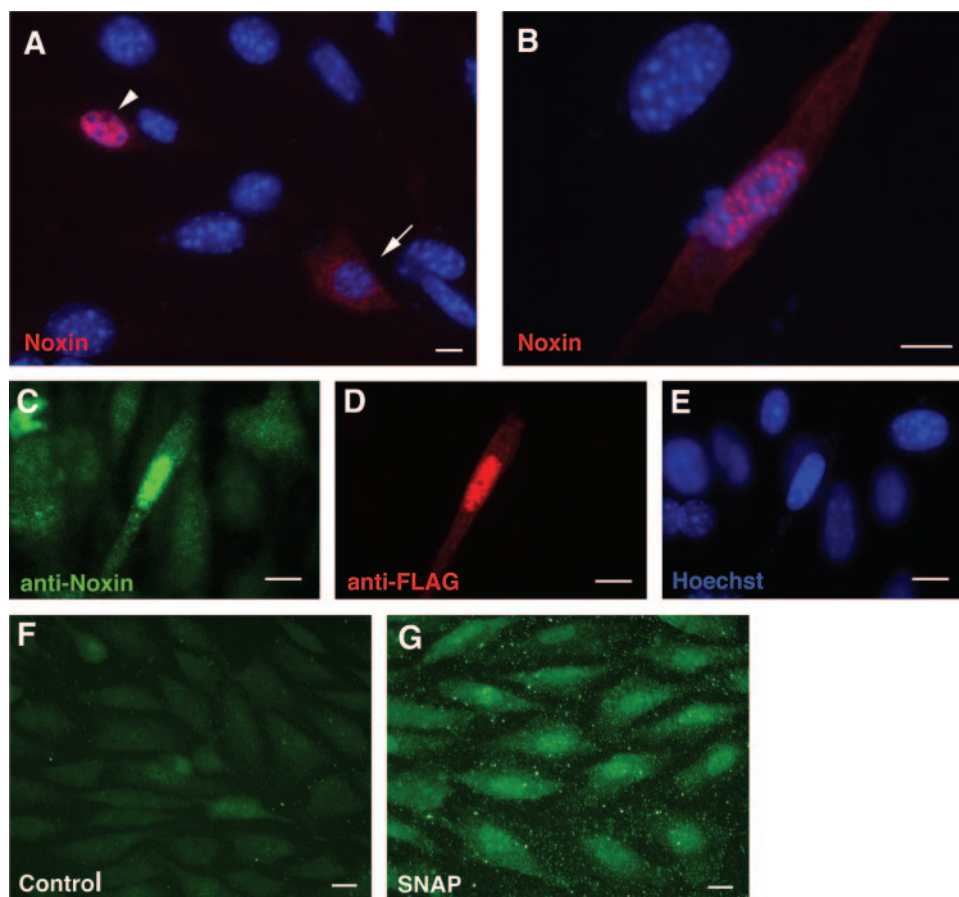
FIG. 3. Subcellular distribution of Noxin. (A and B) NIH 3T3 cells were transfected with pFLAG-noxin. The cells were stained with anti-FLAG antibody (red) and Hoechst 33342 to visualize the nuclei (blue). The FLAG-Noxin protein is present in the cytoplasm (arrow) or in the nucleus (arrowhead) of the transfected cells (A). It is often seen in small subnuclear particles (B). (C to E) Staining of pFLAG-noxin-transfected cells with anti-Noxin antibody (C), anti-FLAG antibody (D), or Hoechst 33342 (E). (F and G) Endogenous Noxin, visualized with an antibody raised against a C-terminal region peptide, is mainly localized in the cytoplasm. Exposure to SNAP results in a predominantly nuclear localization of the protein (note that the quality of the endogenous Noxin signal did not allow us to visualize its precise subnuclear distribution). Scale bars, 5 μm.

spermatocytes, Noxin is localized to the periphery of the nucleus, in a structure which may correspond to the centrosome, the Golgi body, or the XY body of these cells. The expression of Noxin in the testis was also confirmed by Western blots, which showed Noxin expression in the testes from wild-type mice, absence of the protein in the knockouts, and an intermediate level of expression in heterozygous animals (Fig. D, f).

To further determine the subcellular localization of Noxin, we transfected NIH 3T3 cells with a plasmid encoding Noxin tagged with the FLAG epitope at its N terminus (pFLAG-noxin). A majority of the transfected cells showed nuclear localization of Noxin, compatible with the presence of two predicted nuclear localization signals in the Noxin protein (Fig. 3A and B); at the same time, in a number of cells, Noxin was present in the cytoplasm (Fig. 3A). The distributions of the protein were identical whether revealed by the polyclonal antibody to Noxin or by the antibody to the FLAG epitope (Fig. 3C to E). When in the nucleus, Noxin can be seen in subnuclear particles in the euchromatic regions; these Noxin-containing particles did not colocalize with several subnuclear structures revealed with antibodies to PML (a component of

PML bodies), SF2 (a component of spliceosomes), or phospho-H2AX (a DNA repair-related protein) (data not shown).

When the distribution of the endogenous Noxin protein was examined in NIH 3T3 cells, it was found to be localized both to the cytoplasm (predominantly) and to the nucleus (Fig. 3F and G). However, the protein accumulated in the nucleus when cells were exposed to the NO donor SNAP. Together, our results show that Noxin is expressed in primary spermatocytes of the testis, where it is localized to discrete subcellular structures, and that it is also expressed in the fibroblasts and accumulates in the nucleus in response to NO.

***noxin* expression is induced in response to stress in a p53-dependent manner.** *noxin* was identified as an NO-inducible gene, and we determined the time course of its induction by the NO donor SNAP. *noxin* mRNA levels started to increase 2 h after the addition of SNAP and reached maximal levels 8 h after the addition (Fig. 4A). The pattern of *noxin* induction by SNAP was similar to that of a p53-dependent gene, *mdm2*, suggesting that *noxin* expression may be controlled by p53 (note that we have previously shown that in the absence of the p53 gene, the induction of *noxin* by SNAP is reduced [13]).
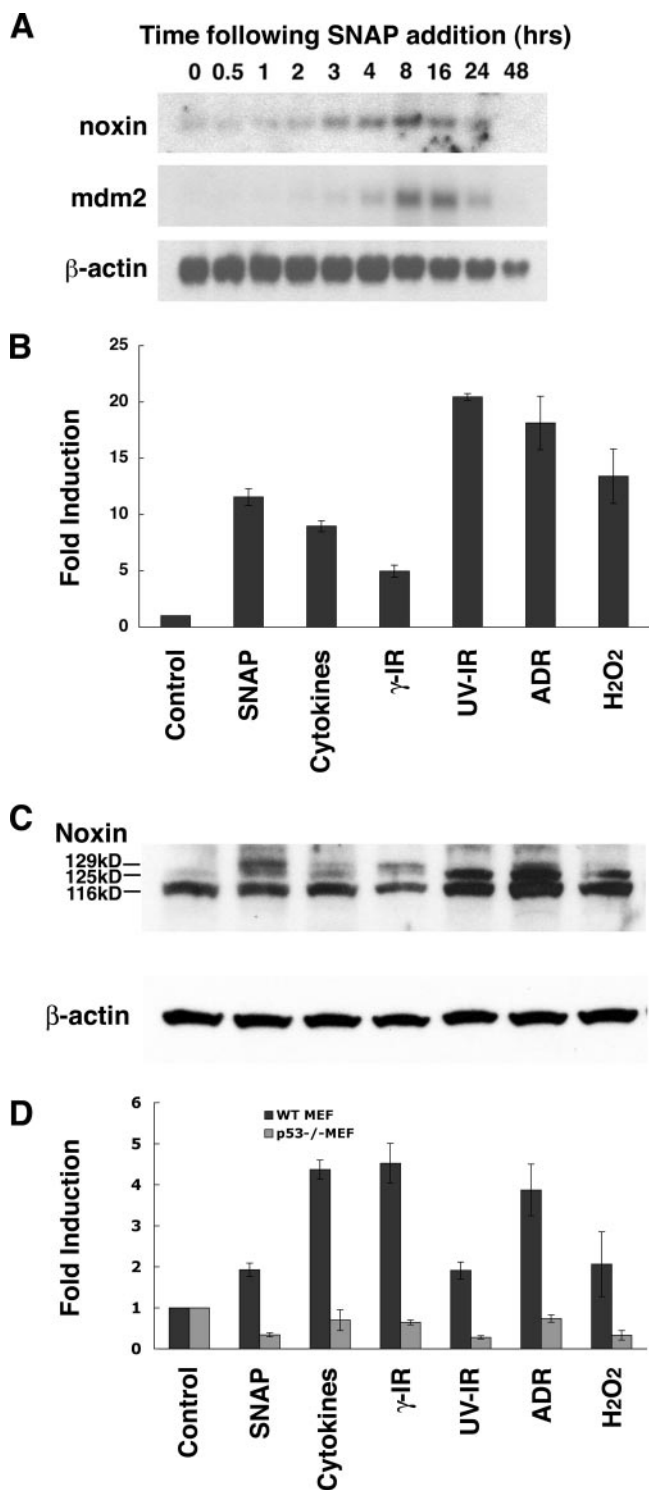
A

Time following SNAP addition (hrs)

0 0.5 1 2 3 4 8 16 24 48

noxin

mdm2

β-actin

B

C

Noxin

129kD—
125kD—
116kD—

β-actin

D

We next examined whether induction of *noxin* is specific to NO or whether *noxin* expression can also be induced by other known stress stimuli. We exposed NIH 3T3 cells to γ-irradiation, UV irradiation, the chemotherapeutic agent adriamycin, and hydrogen peroxide; we also used a mixture of cytokines (TNF-α, IFN-γ, and IL-1β), which is known to be a potent inducer of reactive oxygen and nitrogen species. Each of these treatments resulted in a strong induction of *noxin* mRNA (e.g., 21-fold for the UV irradiation) (Fig. 4B), demonstrating that the *noxin* gene can respond to a wide range of dissimilar stimuli by transcriptional activation, thus characterizing *noxin* as a general stress-responsive gene.

In parallel to the *noxin* mRNA accumulation in response to the stress stimuli, Noxin protein levels were also increased by each of the tested stimuli (Fig. 4C). In unstimulated cells, endogenous Noxin protein is revealed on the Western blot as a major band migrating at 116 kDa and a minor band at 125 kDa. All of the examined stimuli increased the Noxin protein levels, and some (e.g., SNAP, UV irradiation, adriamycin, and H_2O_2) specifically increased the levels of the 125-kDa polypeptide; furthermore, in the SNAP-, cytokine-, γ-irradiation, and adriamycin-treated cells, an additional band of 129 kDa was evident. Together, these results demonstrate that *noxin* mRNA and protein expression is strongly induced by each of the tested stress stimuli and that a specific set of polypeptides (presumably reflecting posttranslational modifications of the serine-rich Noxin protein) is induced in response to each stimulus.

We next examined the contribution of p53 to *noxin* induction by comparing the effect of the stress treatments applied to the NIH 3T3 cells (see above) on *noxin* mRNA expression in MEFs from wild-type and p53$^{-/-}$ animals. Similar to the NIH 3T3 cells, each of these treatments increased the levels of *noxin* expression in MEFs, and in each case, this induction was abrogated by the lack of p53 (Fig. 4D). This confirms the stress-responsive nature of the *noxin* gene and demonstrates that induction of *noxin* in response to stress is dependent on p53.

***noxin* expression is regulated by the cell cycle.** We next examined the possibility that *noxin* expression is related to cell cycle progression. When NIH 3T3 cells were arrested in G_0 phase by serum withdrawal, *noxin* mRNA expression was strongly reduced compared to that in asynchronously dividing cells (Fig. 5A). When the cells were released from cell cycle arrest by the addition of serum, *noxin* mRNA was strongly induced (up to 15-fold) as the cells passed through S and G_2 phases (the status of the cell cycle was determined by flow cytometry) (Fig. 5B). The cell cycle-dependent expression was also evident for the Noxin protein: its levels were lower in the arrested cells than in the asynchronous culture and strongly increased after the addition of serum and progression through the cell cycle (Fig. 5C). The Noxin levels were highest in cells in G_2/M phase; they were also induced by the cell cycle inhib-

FIG. 4. *noxin* mRNA is induced by NO and other stress stimuli in a p53-dependent manner. (A) Northern blot showing the kinetics of *noxin* and *mdm2* mRNA induction by SNAP. Results for β-actin are shown as a control. (B) *noxin* mRNA is induced by a variety of stress stimuli. *noxin* mRNA was quantitated by Q-PCR in samples from NIH 3T3 cells treated for 16 h with SNAP, a cocktail of cytokines (TNF-α, IFN-γ, and IL-1β), γ-irradiation (γ-IR), UV irradiation (UV-IR), adriamycin (ADR), or hydrogen peroxide (H_2O_2). (C) Noxin protein is induced by stress stimuli. NIH 3T3 cells treated with stress stimuli (arranged in the same order as in panel B) were analyzed for the Noxin

protein by Western blotting using anti-Noxin antibody. Noxin appears in three separate bands of 116, 125, and 129 kDa. (D) *noxin* RNA induction by stress stimuli is dependent on p53. p53$^{+/+}$ and p53$^{-/-}$ MEFs were exposed to stress stimuli (the lanes are arranged in the same order as in panel B) and analyzed for *noxin* mRNA expression. The error bars indicate standard errors of the mean.
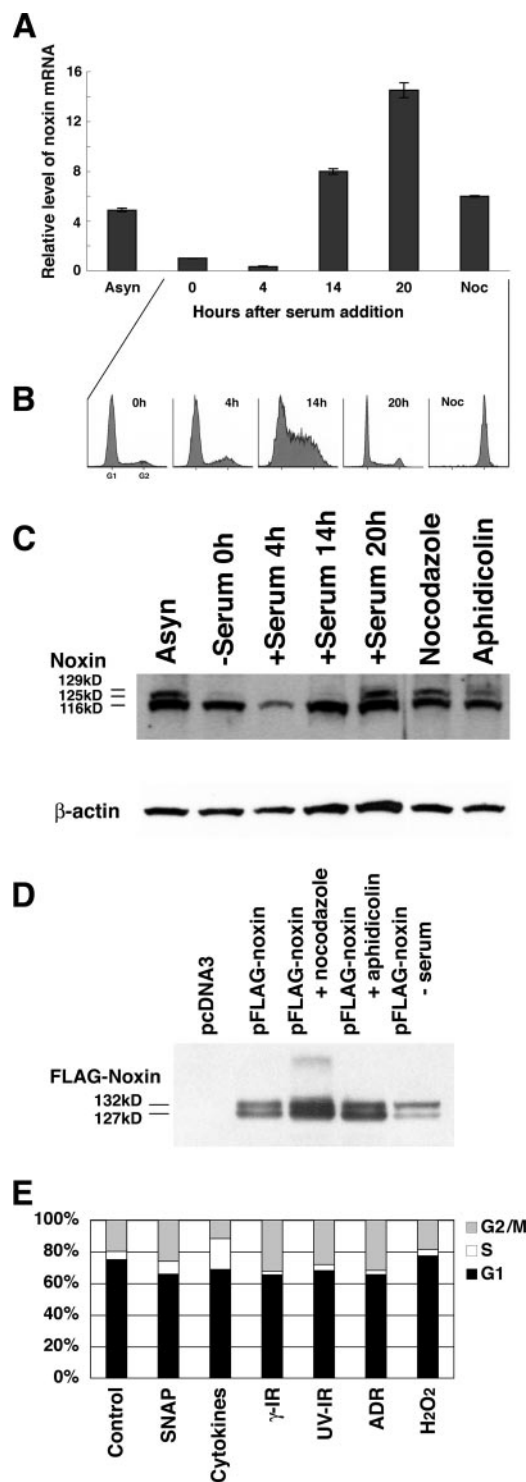
A

B

C

D

E

itors nocodazole and aphidicolin (note that the levels of the minor 125-kDa and 129-kDa bands were selectively increased in response to serum or the inhibitors) (Fig. 5C). Noxin expression was higher in cells treated with nocodazole (which arrests cells in G_2/M phase) than in cells exposed to aphidiciolin or serum withdrawal (which induce S- and G_1-phase arrest, respectively).

High levels of *noxin* mRNA and protein expression in serum- and nocodazole-treated cells in G_2/M phase raise the possibility that the stress-induced expression of *noxin* (Fig. 4) merely reflects accumulation of cells in the G_2/M phase. We examined the cell cycle phase distribution of NIH 3T3 cells exposed to each of the stress stimuli used for the experiments in Fig. 4 and found (i) that each of these stimuli induced a specific pattern of cell cycle phase distribution and (ii) that there was no correlation between the level of *noxin* mRNA induction in response to a certain stimulus and the proportion of cells accumulating in G_2/M phase in response to this stimulus (for instance, the fraction of G_2/M cells after exposure to γ-irradiation was 2.75- and 1.75-fold higher than after exposure to cytokines and H_2O_2, respectively, whereas mRNA levels were 1.5- and 2.5-fold lower; furthermore, the proportion of G_2/M cells following H_2O_2 exposure was similar to that of unstimulated cells, yet the mRNA level was 13-fold higher) (Fig. 5E). Together, our results demonstrate that Noxin expression is controlled by the cell cycle and suggests a possibility that Noxin may interact with the cell cycle machinery.

Noxin can induce cell cycle arrest. To examine the possibility that Noxin may affect cell cycle progression, we transfected NIH 3T3 cells with plasmids encoding FLAG-Noxin, p21/WAF, p53, or p53dn. In addition, as controls, we used constructs coding for cyan fluorescent protein with a nuclear localization signal (CFP-nuc), yellow fluorescent protein fused to actin (YFP-actin), or vector construct alone. We next labeled cells with BrdU for 24 h and analyzed the cells in situ by immunocytochemistry for BrdU and Noxin (or the other listed proteins) (Fig. 6A and B). We then determined the fraction of BrdU-positive cells among the cells that expressed the recombinant protein (transfected cells) and among the cells that did not receive the transgene and did not express the recombinant protein (untransfected cells). Comparison of these fractions showed that Noxin was highly effective in suppressing DNA synthesis in transfected cells (24% of the value for the untransfected cells) (Fig. 6B). p21/WAF and p53 were also effective in suppressing DNA synthesis in cells that received these genes (39% and 68% of the values for the untransfected cells, respectively), whereas CFP-nuc and YFP-actin (taken as con-

FIG. 5. *noxin* mRNA levels are regulated by the cell cycle. (A) NIH 3T3 cells, synchronized by serum starvation (DMEM with 0.5% serum for 24 h) were released from arrest by the addition of 10% serum (corresponding to the zero hour time point). *noxin* mRNA expression was analyzed using Q-PCR 0, 4, 14, or 20 h after the addition of serum. Asyn, cells growing asynchronously; Noc, G_2/M-arrested cells after treatment with nocodazole for 20 h. The error bars indicate standard errors of the mean. (B) In parallel, cell cycle distribution was determined by PI staining and flow cytometry analysis; this confirmed that cells progress through the cell cycle phases (0- to 20-h time points) or accumulate in G_2/M (nocoda

zole). (C) Masses of Noxin protein determined by Western blotting. (D) After transfection with pFLAG-noxin or pcDNA3 vector, cell division was arrested with three different treatments (nocodazole, aphidicolin, or a low concentration of serum). Recombinant protein was detected on a Western blot using the anti-FLAG antibody. FLAG epitope increases the electrophoretic mobility of the recombinant protein. (E) Cell cycle distribution of stress-exposed NIH 3T3 cells. The cells were fixed with 70% ethanol for 16 h after stress treatment, and the cell cycle distribution was determined by PI staining and flow cytometry analysis. The segments of the bars depict the proportion of cells in G_1 (black), S (white), and G_2/M (gray) phases of the cell cycle.
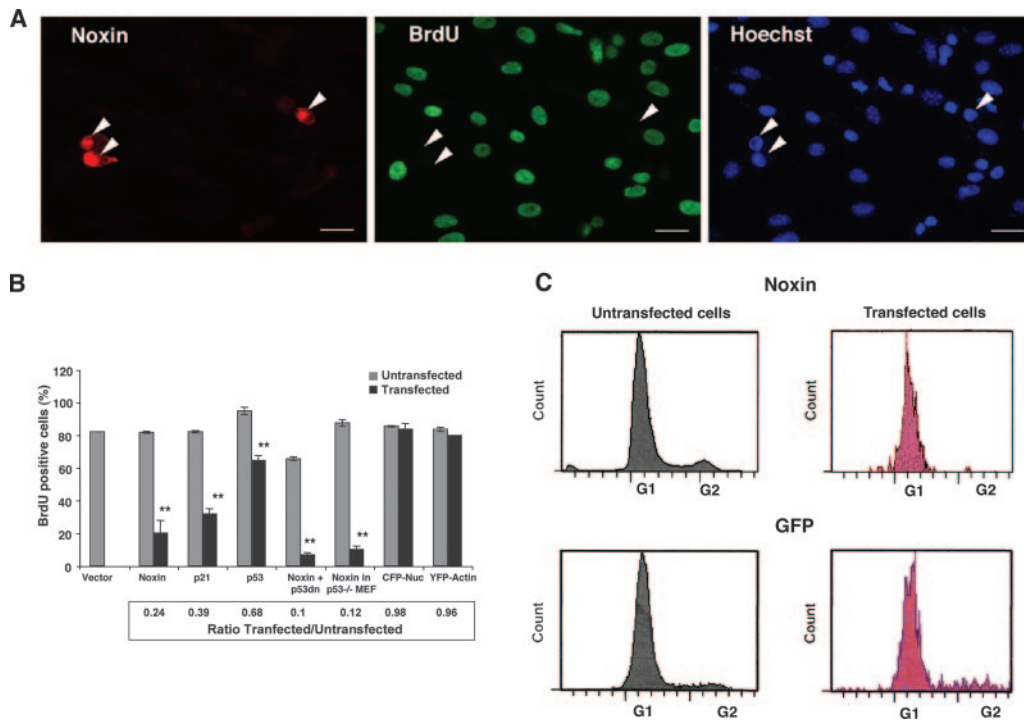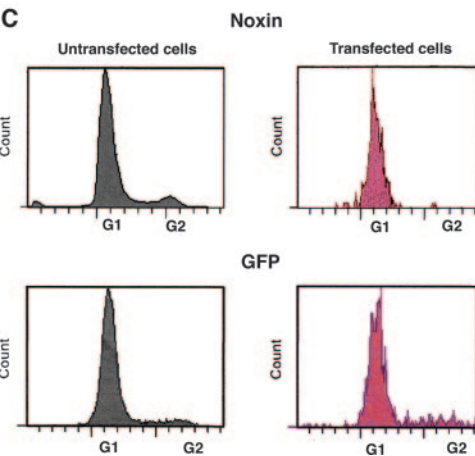
FIG. 6. Ectopic expression of Noxin induces G_1 cell cycle arrest. (A) NIH 3T3 cells were transfected with pFLAG-noxin and cultured in medium containing BrdU for 24 h. The cells were fixed and stained with anti-FLAG (red) and anti-BrdU (green) antibodies; Hoechst 33342 (blue) was used for nuclear counterstaining. (B) The fractions of BrdU-labeled cells among the cell populations were determined for cells that express or do not express the transfected gene. Similar experiments were performed using constructs for p21/WAF, p53, p53dn, CFP-Nuc, and YFP-actin. The ratios of these fractions for transfected and untransfected cells are shown below the graph. Noxin action was also analyzed in p53-deficient MEFs. The error bars indicate standard errors of the mean. (C) Cells transfected with pFLAG-noxin were stained with anti-FLAG antibody and FITC-conjugated anti-mouse IgG antibody after permeabilization. Cell cycle distributions of untransfected and transfected cells were analyzed by DAPI staining and flow cytometry.

trols) did not show any effect on DNA synthesis in transfected cells (98% and 96%, respectively). To determine whether the activity of p53 is required for the action of Noxin, we contransfected Noxin with a dominant-inhibitory version of p53; this did not affect the ability of Noxin to induce cell cycle arrest. Similarly, Noxin was effective in suppressing DNA synthesis in MEFs from p53-deficient mice. Together, these data show that Noxin expression can induce cell cycle arrest and that this action of Noxin does not require the activity of p53.

To determine the phase of the cell cycle affected by Noxin, we transfected the NIH 3T3 cells with pFLAG-noxin- or GFP-expressing recombinant plasmids and used flow cytometry following anti-FLAG staining and GFP fluorescence to compare the DNA distribution in cells that expressed or did not express the *noxin* transgene (Fig. 6C). Most of the pFLAG-noxin-transfected cells had 2n DNA content, whereas untransfected cells showed the usual distribution, with a fraction of cells having a 4n DNA set. In control experiments, cells that received or did not receive the GFP construct upon transfection did not show any changes in the cell cycle distribution pattern. This suggests that cells which express the transfected *noxin* gene are arrested in G_1 or early S phase.

Although our experiments with dominant-inhibitory p53 and with $p53^{-/-}$ MEFs (Fig. 6B) indicated that Noxin does not require p53 to induce cell cycle arrest, we examined whether Noxin expression can affect the cellular levels of p53. We

transfected cells with pFLAG-noxin- or GFP-expressing plasmids and determined the levels of p53 using immunocytochemistry and flow cytometry. p53 levels were increased only in the cells that received the *noxin* gene but not in cells that did not show expression of Noxin or in cells that received the GFP gene (Fig. 7A and B). Thus, expression of Noxin elevates the cellular levels of p53 and is itself induced in a p53-dependent manner; however, Noxin does not require p53 to induce cell cycle arrest.

Knockout of the *noxin* gene and the phenotype analysis of *noxin* knockout mice. For further insights into the potential function of Noxin, we decided to produce a targeted deletion within the *noxin* gene. We targeted exon 6 of the gene, since a large part of murine Noxin is encoded by this exon (Fig. 8A and B). Replacement of these sequences with the neomycin phosphotransferase gene inactivated the *noxin* gene so that *noxin* mRNA could not be detected in the tissues of mice carrying a homozygous deletion of the gene or in the embryonic fibroblasts derived from these knockout mice. Mice carrying one mutant *noxin* allele produced approximately half as much *noxin* mRNA as the wild-type animals (Fig. 8C). *noxin* heterozygotes produced homozygous mutant progeny at a normal Mendelian ratio, and the homozygous animals were born with a normal ratio of male to female mice. Homozygous *noxin* mutants were viable and fertile, developed without growth retardation, and displayed no detectable abnormalities on
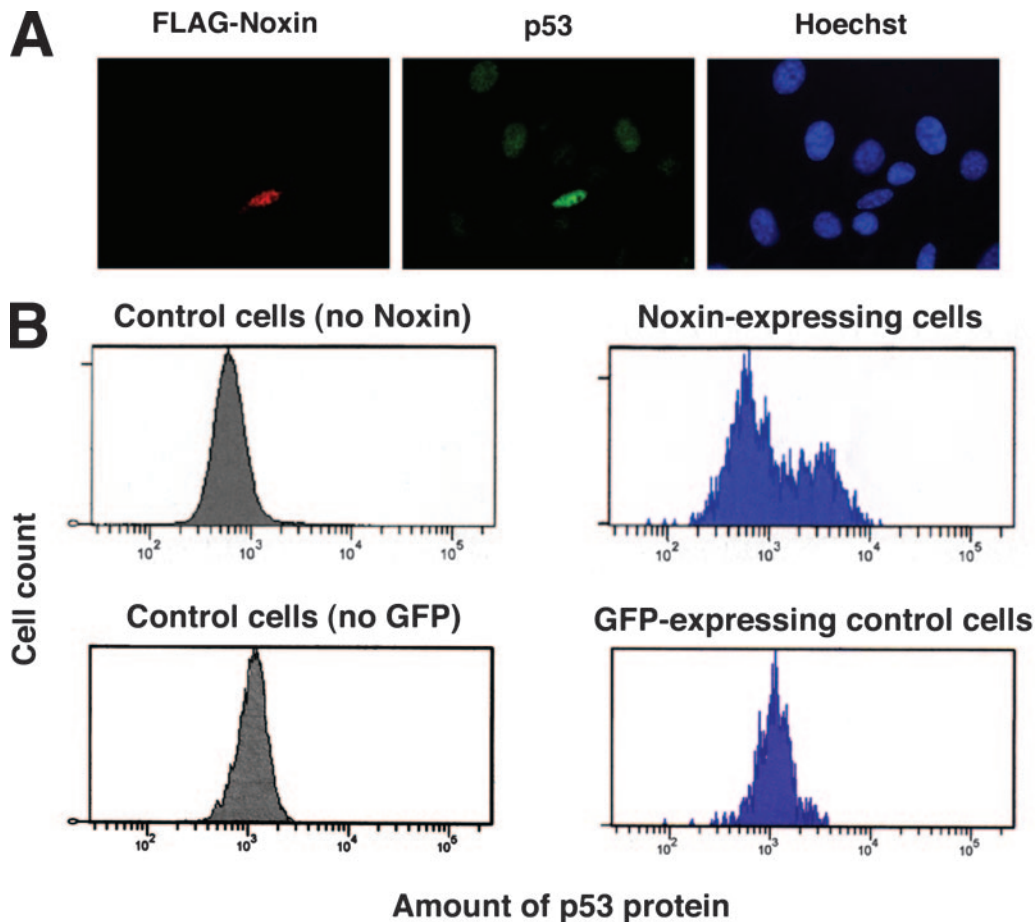
FIG. 7. p53 upregulation in NIH 3T3 cells transfected with Noxin. (A) Cells transfected with pFLAG-noxin were stained with anti-FLAG and anti-p53 primary antibodies and ALEXA Fluor 596- and 488-conjugated secondary antibodies, respectively. Cells expressing Noxin (red) showed higher levels of p53 (green) than cells that did not express Noxin. (B) Cells transfected with pFLAG-noxin (top) and pEGFP (taken as a control; bottom) were stained with anti-FLAG and anti-p53 primary antibodies and PE- and FITC-conjugated secondary antibodies. Then, Noxin-FLAG- or EGFP-negative (left) and -positive (right) cells were analyzed for the amount of p53 protein by using flow cytometry.

visual inspection and macroscopic analysis of the visceral organs. One notable exception was the heart, which was larger in the knockout animals (Table 1).

We further analyzed the structure of the testis, the major site of Noxin expression. Testes of Noxin-deficient animals did not show detectable differences in weight, diameter of seminiferous tubules, or number of primary spermatocytes (Table 1). However, we found a significant decrease in the number of round spermatids in Noxin-deficient animals (Table 1).

Since the bone marrow and spleen are among the major sites of Noxin expression, we examined whether hematopoiesis was affected by disruption of the *noxin* gene We compared the composition of blood and the content of hematopoietic progenitors in the bone marrow and spleens of homozygous knockout animals and their heterozygous and wild-type littermates. We did not see significant differences in the blood cell profile in peripheral blood, spleen, or bone marrow; in the cellularity of the spleen or bone marrow; in the number of CFC-8d and CFC-12d cells in the bone marrow; or in the number of CFC-12d colonies in the spleen. We were able, however, to detect differences in the number of CFC-8d cells in the spleens of homozygous knockouts (12% increase; $P <$

0.05) and Sca1-positive cells in the bone marrow (a 45.5% decrease; $P < 0.001$). Thus, we could detect only a few significant differences between the wild-type and knockout mice in a wide range of hematopoiesis-related parameters.

Since Noxin responds to various stress stimuli, we decided to test the response of *noxin* mutant mice to lipopolysaccharide-induced endotoxic shock. Lipopolysaccharide challenge induces oxidative and nitrosative stress and, at high doses, results in mortality. We compared the response of the wild-type $noxin^{+/+}$ mice with those of their littermates carrying a homozygous or a heterozygous deletion of the *noxin* gene and could not find differences in mortality between the three genotypes; it is possible that the threshold for detecting the differences between the wild-type and *noxin* knockout mice was not achieved.

Cell death is increased by *noxin* gene ablation or down regulation. Since Noxin can induce cell cycle arrest and, in addition, responds to various types of stress stimuli, including NO, we compared the growth characteristics of MEFs isolated from $noxin^{-/-}$ animals or their wild-type ($noxin^{+/+}$) littermates. We either left cells untreated or exposed them to the NO donor SNAP and then labeled the cells with BrdU; col-
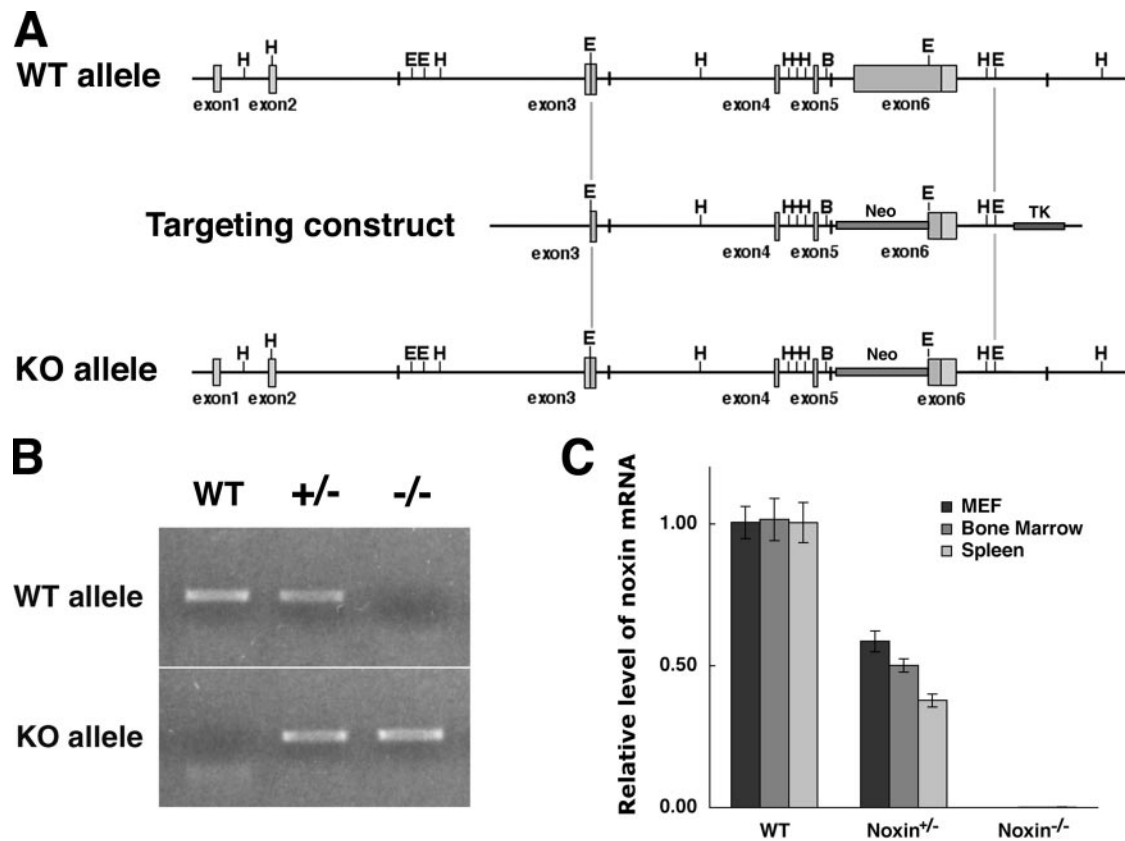
FIG. 8. Targeted inactivation of the *noxin* gene. (A) A part of exon 6 (the longest exon) in the *noxin* gene was replaced with a cassette containing a neomycin resistance gene (B, BamHI; E, EcoRI; H, HindIII). (B) Genomic DNA of mutant mice was analyzed by PCR using specific primer sets corresponding to the eliminated exon 6 (WT) and to the targeting cassette (KO). Wild-type or knockout mice carry only one type of allele (WT or KO), while heterozygote mice have both alleles. (C) Total RNAs extracted from MEFs, adult bone marrow, and spleen were analyzed by Q-PCR for the expression of *noxin* mRNA. Tissues from *noxin*$^{+/-}$ (heterozygous) mice expressed approximately half as much *noxin* mRNA as wild-type mice. *noxin* mRNA was not detected in tissues from *noxin*$^{-/-}$ mice. The error bars indicate standard errors of the mean.

lected aliquots after 4, 16, and 22 h; and performed bivariate DNA analysis using flow cytometry. Such analysis provides detailed information on how cells progress through the cell cycle, with a particular emphasis on the S phase. We could not reveal noticeable differences in how the wild-type or mutant cells traverse the S phase in the absence of NO (Fig. 9A). The effect of SNAP on cells was dramatic, decreasing the fraction of dividing cells by 95.5%; however, we did not detect any differences between the responses of the wild-type versus the mutant cells when analyzing either the fraction of cells in the S phase or the kinetics of response to SNAP (Fig. 9A). Thus, inactivation of the *noxin* gene does not noticeably affect the rate of DNA synthesis or the response of cells to NO.

We noticed, however, that the fraction of sub-G$_1$ cells was higher in Noxin-deficient cells. At each time point analyzed, this fraction was higher in *noxin*$^{-/-}$ than in *noxin*$^{+/+}$ MEFs (13.8, 16.3, and 11.5 versus 9.7, 5.1, and 3.5%, respectively) (Fig. 9B, fraction P6); incubation with SNAP did not noticeably affect this fraction in the *noxin*$^{+/+}$ or *noxin*$^{-/-}$ cells. Since the sub-G$_1$ fraction corresponds to dying cells that have lost part of their DNA, these data suggest that lack of Noxin increases the fraction of cells that undergo apoptosis. We further tested this possibility by using alternative assays for apoptosis, measuring annexin V$^+$ PI$^-$ cells (Fig. 9C and D) and TUNEL-positive cells (Fig. 9E) among *noxin*$^{+/+}$ and *noxin*$^{-/-}$ cells. The results of these assays showed that *noxin*$^{-/-}$ MEFs had signif-

TABLE 1. Tissue weights and parameters in testes from wild-type and *noxin*$^{-/-}$ mice[a]

Genotype	Tissue wt[b]			Values for parameters in testes		
	Heart	Spleen	Testis	Seminiferous tubule diam (μm)	Spermatocytes[c]	Spermatids[c]
Wild type	4.32 ± 0.10	2.70 ± 0.17	2.83 ± 0.20	235.30 ± 2.66	54.51 ± 1.00	115.60 ± 1.94
noxin$^{-/-}$	4.87 ± 0.18*	2.88 ± 0.28	2.48 ± 0.11	230.49 ± 2.69	52.18 ± 1.06	107.65 ± 1.98**

[a] Shown are values ± standard errors. *, $P < 0.05$; **, $P < 0.01$.
[b] Milligram weight of organ per gram mouse body weight.
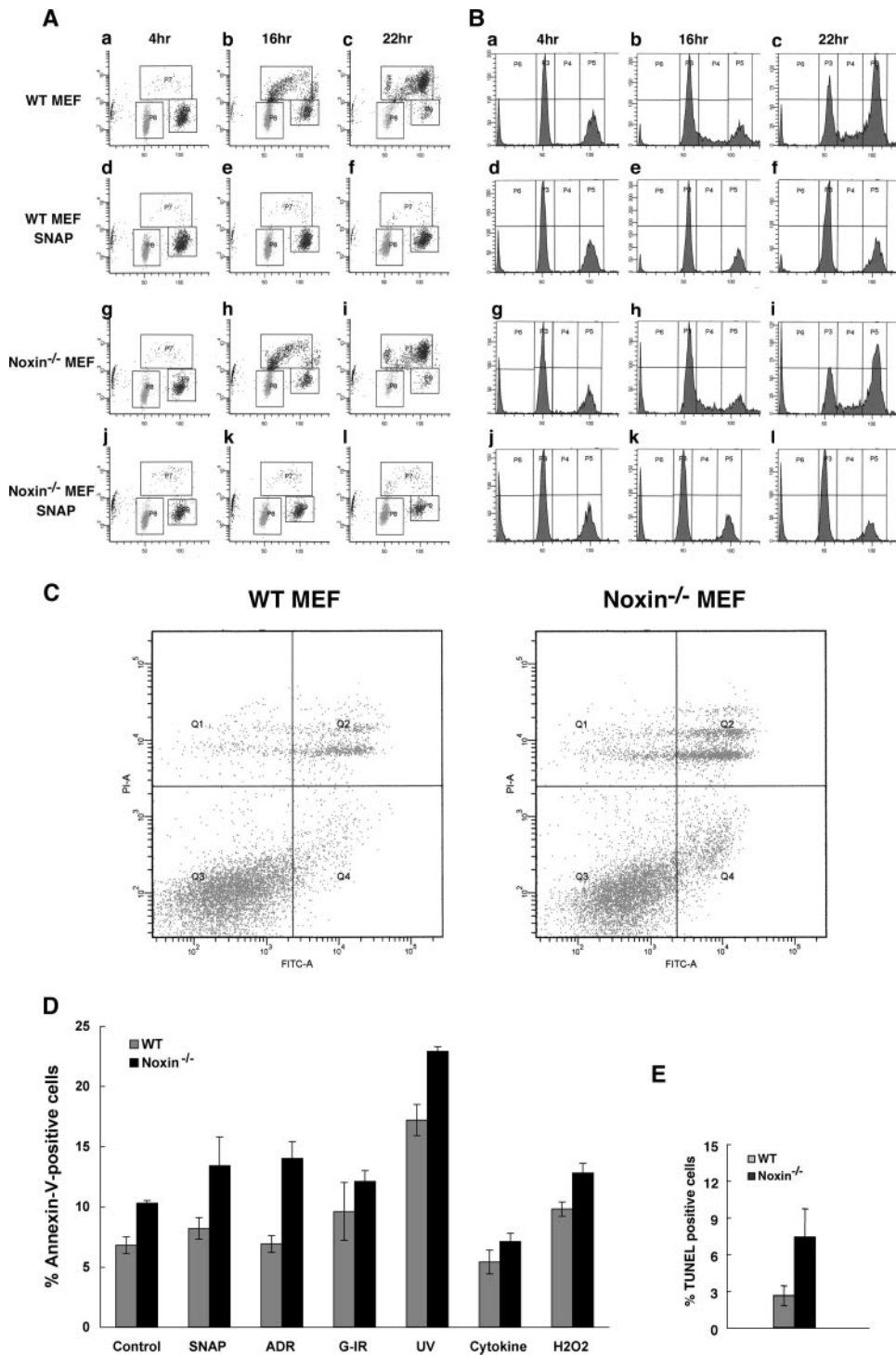[c] Number of cells in a cross section of tubule.

FIG. 9. MEFs isolated from *noxin*$^{-/-}$ mice have normal growth and response to SNAP treatment but increased cell death. (A and B) MEFs from wild-type (WT) and *noxin*$^{-/-}$ mice were arrested with low-serum (0.1%) culture medium for 24 h and released by adding 10% serum. At the time of release, BrdU was added to the culture medium and the cells were further incubated for 4, 16, or 22 h (as indicated). Cells were collected, stained with PI, and analyzed by flow cytometry for BrdU-positive cells (*x* axis, PI; *y* axis, BrdU) (A) and for cell cycle distributions (*x* axis, PI; *y* axis, number of cells) (B). (Populations: P3, G$_1$; P4, S; P5, G$_2$/M; P6, sub-G$_1$). The growth of *noxin*$^{-/-}$ MEFs under normal conditions (A, g to i) and after the addition of SNAP (A, j to l) were similar to that of wild-type MEFs (A, a to c and d to f). However, *noxin*$^{-/-}$ MEFs contained a larger fraction of cells in sub-G$_1$ phase. (C to E) Wild-type and *noxin*$^{-/-}$ MEFs were grown in normal culture medium or treated with the previous panel of stress stimuli (SNAP, cytokines, UV irradiation, γ-irradiation, adriamycin, or hydrogen peroxide) for 16 h. Cells were collected and assayed for annexin V-positive cells (C and D) and TUNEL-positive cells (E). Annexin V$^+$ PI$^-$ cells were quantified by flow cytometry (*x* axis, annexin V; *y* axis, PI). (Q1, annexin V$^-$ PI$^+$; Q2, annexin V$^+$ PI$^+$; Q3, annexin V$^-$ PI$^-$; Q4, annexin V$^+$ PI$^-$). Examples are shown for untreated wild-type MEFs and Noxin-deficient MEFs (C). The graph shows the percentage of annexin V$^+$ PI$^-$ cells (Q4) for each of the stress stimuli tested (D). The number of TUNEL-positive cells is expressed as a percentage of the total cell population (E). The data shown in the bar graphs represent the means ± standard errors.
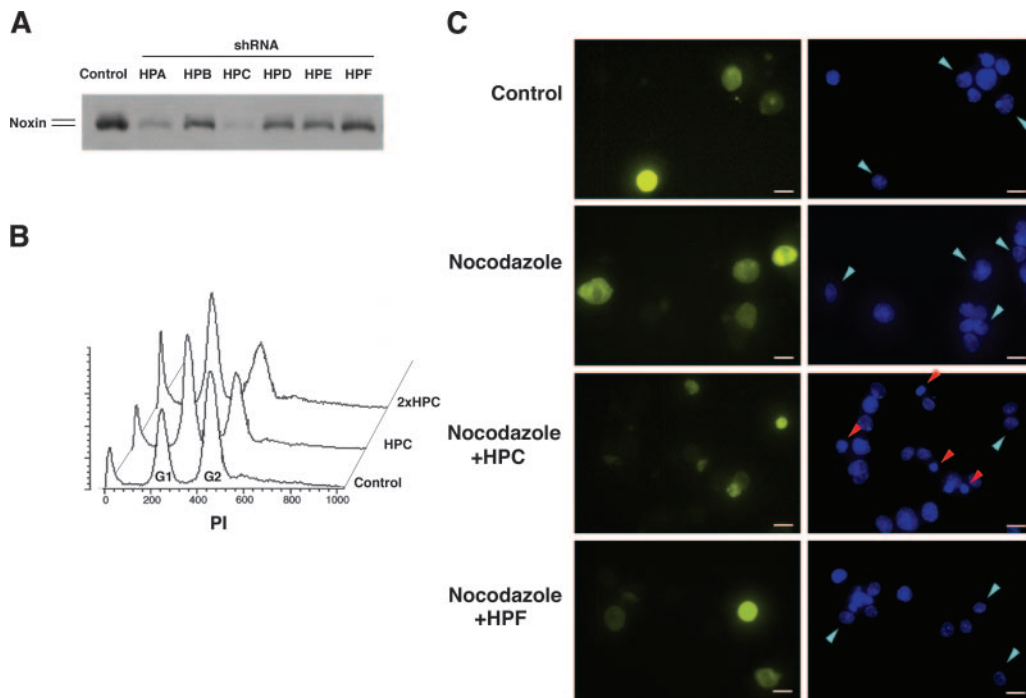
FIG. 10. *noxin* knockdown by shRNA increases the fraction of apoptotic cells after treatment with nocodazole. (A) Selection of shRNA constructs. Six different shRNA constructs (HPA to HPF) were produced and examined for their abilities to suppress the expression of Noxin protein. NIH 3T3 cells were cotransfected with constructs coding for Noxin shRNAs, FLAG-Noxin, and luciferase, and the lysates were examined for luciferase expression. After normalization, protein samples were analyzed by Western blotting for the expression of FLAG-Noxin protein. The HPC hairpin construct showed the strongest inhibition of Noxin expression, whereas HPF had no effect and was used as a control. (B) NIH 3T3 cells were transfected with 1 μg (HPC) or 2 μg (2× HPC) of the HPC shRNA construct, treated with nocodazole for 20 h, collected, stained with PI, and analyzed for DNA content using flow cytometry. Nocodazole treatment resulted in accumulation of cells in the G_2/M phases. Transfection with HPC decreased the fraction of cells in G_2/M while increasing the sub-G_1 population. (C) Cells were cotransfected with the HPC or HPF shRNA constructs, together with the YFP-actin construct, and stained with Hoechst stain. shRNA-transfected cells were identified by YFP expression. HPC-transfected cells (yellow) showed condensed chromatin structures, corresponding to apoptotic cells (red arrowheads). The nuclei of cells transfected with HPF and YFP-actin or with YFP-actin alone and the nuclei of nontransfected cells had normal shape (light-blue arrowheads). Scale bars, 10 mm.

icantly larger numbers of apoptotic cells (140% by the annexin assay and 285% by the TUNEL assay) than their wild-type counterparts (Fig. 9D and E).

Furthermore, we applied the annexin assay for apoptosis to $noxin^{+/+}$ MEFs subjected to the panel of treatments described above: SNAP, γ-irradiation, UV irradiation, adriamycin, hydrogen peroxide, and cytokines. For each type of stress, the fraction of apoptotic cells was higher in Noxin-deficient MEFs than in their wild-type counterparts (Fig. 9D). Together, these three assays (DNA content measurement, TUNEL, and annexin V/PI flow cytometry) indicate that lack of Noxin increases the rate of programmed death in cells under normal conditions or when challenged with stressful stimuli.

To further confirm this notion, we probed the role of Noxin in normal cells by down regulating its expression using the RNA interference approach. We generated six shRNA constructs, which corresponded to different regions of *noxin* mRNA, and compared their efficiencies by coexpressing them with recombinant *noxin* cDNA (Fig. 10A). The shRNA construct that showed the highest efficiency in this assay (HPC) was used to transfect NIH 3T3 cells treated with nocodazole (to arrest the cells in the G_2/M phase). The downregulation of Noxin using this shRNA construct decreased the fraction of cells in G_2/M and increased the fraction of cells in the sub-G_1

population: 5.7 ± 0.4% in control cells versus 7.8 ± 1.3% in cells transfected with 1 μg of HPC and 8.0 ± 1.7% in cells transfected with 2 μg of HPC (Fig. 10B). Furthermore, cells transfected with HPC often showed condensed nuclei characteristic of apoptotic cells (Fig. 10C). Taken together, this series of experiments indicated that Noxin acts as an anti-apoptotic factor and that its absence increases cell death under normal and stress conditions.

DISCUSSION

Here, we describe *noxin*, a new stress-induced gene, and a mutant mouse line in which this gene is inactivated. *noxin* mRNA and protein expression is controlled by the cell cycle; it can also be activated by a wide range of stress stimuli. Noxin plays an anti-apoptotic role, so that when the *noxin* gene is inactivated or downregulated, cells exhibit significantly higher levels of apoptosis than their counterparts with normal levels of Noxin. This is evident under basal conditions and is maintained when cells are challenged by a range of dissimilar stress stimuli. Thus, our data suggest that *noxin* is a general stress response gene whose expression is related to the cell cycle and whose product may be important to prevent cell death under a wide range of conditions.

We had initially identified *noxin* as an NO-inducible gene, and indeed, it is activated by NO donors to a greater degree than any other tested gene related to cell cycle progression, cell death, or stress response (reference 13 and data not shown). Its induction by SNAP is prevented by the deletion of the p53 gene, indicating that p53 is important for the expression of *noxin. noxin* expression is induced both by chemical NO donors and by in vivo stimuli that induce NO production, e.g., cytokines; in the latter case, induction of *noxin* is dependent on the activity of NOS and can be prevented by NOS inhibitors (reference 13 and unpublished results).

In addition to NO and cytokines, *noxin* is induced by a wide range of stimuli: γ-irradiation, UV irradiation, adriamycin, and hydrogen peroxide. These agents activate different immediate targets but converge on a relatively small number of effectors, which can slow down or halt the cell cycle, suppress cell death pathways, and permit the repair process to proceed; alternatively, these effectors may activate the cell death program to eliminate defective cells. We propose that Noxin is a component of the basic cell machinery that is activated by various stressors, helps cells to withdraw from cycling, and prevents cell death.

The idea that Noxin acts as a part of the stress response system is strongly supported by our finding that a decrease or loss of Noxin leads to increased cell death. This was evident in three different types of assays (TUNEL, flow cytometry, and annexin V/PI staining) and in all tested settings, whether using cells from wild-type or *noxin* knockout animals or cells with RNA interference-induced downregulation of *noxin* expression (Fig. 9 and 10). The possible link to stress response is further supported by the presence, in the Noxin molecule, of phosphorylation sites for the ATM, DNA-PK, and Akt kinases, each of which plays a critical role in the stress response (12, 16, 23, 26). This link is also supported by the fact that for each stress stimulus, induction of Noxin was dependent on p53 (Fig. 4D). Furthermore, Noxin's participation in the stress response is compatible with the finding that it accumulates in the nucleus in response to stress. At the same time, since it takes several hours after the introduction of the stressor for the full induction of *noxin*, and since this induction is dependent on p53, it is conceivable that Noxin does not participate in the first line of defense against stress (e.g., compared with p53, whose rapid involvement in the repair process is achieved via posttranslational modification and increased stability of preexisting protein stores) (12, 23).

The possible role of Noxin as a component of the cellular stress response system is further supported by its ability to induce cell cycle arrest (Fig. 6). Ectopic expression of Noxin is as, or more, effective than expression of the cell cycle inhibitors p21/WAF and p53 in inducing cell cycle arrest. It forces the cells to stall in G_1/S, perhaps helping the cells to activate their repair systems. Noxin was effective in inducing cell cycle arrest even in the absence of p53 activity (in $p53^{-/-}$ MEFs or when cotransfected with a dominant-negative p53 construct), indicating that it acts downstream or independently of p53. Note, however, that Noxin induction is dependent on p53 and that Noxin can, in turn, induce p53 levels. This suggests a model in which stress stimuli, in a p53-dependent manner, induce expression of Noxin, which then induces cell cycle arrest and

elevates the levels of p53; the latter, however, is not required for the antiproliferative action of Noxin.

In addition to its ability to control cell cycle progression, Noxin is itself controlled by the cell cycle: the amount of *noxin* mRNA is very small in resting cells but increases almost 50-fold as the cells progress through S phase. In addition, its levels are decreased when cells are arrested by serum deprivation. Furthermore, *noxin* mRNA is mainly expressed in tissues that contain actively proliferating cell populations, such as bone marrow, spleen, and testis; also, it is expressed at much higher levels in actively dividing NIH 3T3 cells than in slowly dividing MEFs. The presence of Noxin may be required in dividing cells to help protect them from stress and damage.

Although we clearly saw the consequences of the loss of the *noxin* gene in cultured cells, we were able to see only small changes in knockout animals (e.g., heart size, the level of Sca1$^+$ cells, and the number of round spermatids). So far, we have been unable to reveal the effect of deleting the gene on the animals' response to stress, e.g., to endotoxic shock; perhaps the loss of the *noxin* gene has a more subtle effect and other stress survival paradigms are required to reveal its contribution. Noxin also seems to be dispensable for the maintenance of the tissues and organs where it is expressed at high levels (testis, spleen, and bone marrow). It may require a focused challenge to these organs to reveal the role of Noxin as a stress response agent. Intriguingly, primary spermatocytes are more resistant to NO-induced apoptosis than other types of cells involved in spermatogenesis, e.g., spermatids (7). This is compatible with our observations that Noxin is selectively expressed in primary spermatocytes and that in the knockout animals, the number of TUNEL-positive cells in the seminiferous tubules is increased (data not shown) and is accompanied by a decrease in the number of spermatids. These observations suggest that Noxin may contribute to the protection of the germ line cells from nitrosative stress or other types of insults.

In conclusion, we cloned a novel gene that is controlled by the cell cycle; is activated in response to nitrosative, oxidative, and other types of stresses; is able to induce cell cycle arrest when ectopically expressed; and acts to counteract apoptotic stimuli, so that its loss results in an increased level of cell death. Our results suggest that Noxin may be a part of the machinery that protects cells during stress by helping them to withdraw from the cell cycle and repair the damage. Noxin may thus directly participate in the repair process and may even be a part of the protein complexes that restore the integrity of the genome after insult and stress.

REFERENCES

1. **Bakkenist, C. J., and M. B. Kastan.** 2004. Initiating cellular stress responses. Cell **118:**9–17.
2. **Bartek, J., and J. Lukas.** 2001. Mammalian G_1- and S-phase checkpoints in response to DNA damage. Curr. Opin. Cell Biol. **13:**738–747.
3. **Boehning, D., and S. H. Snyder.** 2003. Novel neural modulators. Annu. Rev. Neurosci. **26:**105–131.
4. **Brüne, B.** 2003. Nitric oxide: NO apoptosis or turning it ON? Cell Death Differ. **10:**864–869.
5. **Contestabile, A., and E. Ciani.** 2004. Role of nitric oxide in the regulation of neuronal proliferation, survival and differentiation. Neurochem. Int. **45:**903–914.
6. **Decimo, D., E. Georges-Labouesse, and P. Dolle.** 1995. In situ hybridization of nucleic acid probes to cellular RNA, p. 183–210. *In* B. D. Hames and S. J. Higgins (ed.), Gene probes 2: a practical approach, vol. 2. Oxford University Press, New York, NY.
7. **Di Meglio, S., F. Tramontano, G. Cimmino, R. Jones, and P. Quesada.** 2004. Dual role for poly(ADP-ribose)polymerase-1 and -2 and poly(ADP-ribose)-glycohydrolase as DNA-repair and pro-apoptotic factors in rat germinal cells exposed to nitric oxide donors. Biochim. Biophys. Acta **1692:**35–44.
8. **Enikolopov, G., J. Banerji, and B. Kuzin.** 1999. Nitric oxide and *Drosophila* development. Cell Death Differ. **6:**956–963.
9. **Estrada, C., and M. Murillo-Carretero.** 2005. Nitric oxide and adult neurogenesis in health and disease. Neuroscientist **11:**294–307.
10. **Gibbs, S. M.** 2003. Regulation of neuronal proliferation and differentiation by nitric oxide. Mol. Neurobiol. **27:**107–120.
11. **Gudkov, A. V., and E. A. Komarova.** 2003. The role of p53 in determining sensitivity to radiotherapy. Nat. Rev. Cancer **3:**117–129.
12. **Harris, S. L., and A. J. Levine.** 2005. The p53 pathway: positive and negative feedback loops. Oncogene **24:**2899–2908.
13. **Hemish, J., N. Nakaya, V. Mittal, and G. Enikolopov.** 2003. Nitric oxide activates diverse signaling pathways to regulate gene expression. J. Biol. Chem. **278:**42321–42329.
14. **Hofseth, L. J., S. Saito, S. P. Hussain, M. G. Espey, K. M. Miranda, Y. Araki, C. Jhappan, Y. Higashimoto, P. He, S. P. Linke, M. M. Quezado, I. Zurer, V. Rotter, D. A. Wink, E. Appella, and C. C. Harris.** 2003. Nitric oxide-induced cellular stress and p53 activation in chronic inflammation. Proc. Natl. Acad. Sci. USA **100:**143–148.
15. **Ignarro, L. J.** 2000. Nitric oxide: biology and pathobiology. Academic Press, San Diego, CA.
16. **Kastan, M. B., and J. Bartek.** 2004. Cell-cycle checkpoints and cancer. Nature **432:**316–323.
17. **Li, C.-Q., and G. N. Wogan.** 2005. Nitric oxide as a modulator of apoptosis. Cancer Lett. **226:**1–15.
18. **McLaughlin, L. M., and B. Demple.** 2005. Nitric oxide-induced apoptosis in lymphoblastoid and fibroblast cells dependent on the phosphorylation and activation of p53. Cancer Res. **65:**6097–6104.
19. **Nathan, C.** 2003. Specificity of a third kind: reactive oxygen and nitrogen intermediates in cell signaling. J. Clin. Investig. **111:**769–778.
20. **Packer, M. A., Y. Stasiv, A. Benraiss, E. Chmielnicki, A. Grinberg, H. Westphal, S. A. Goldman, and G. Enikolopov.** 2003. Nitric oxide negatively regulates mammalian adult neurogenesis. Proc. Natl. Acad. Sci. USA **100:**9566–9571.
21. **Paddison, P. J., A. A. Caudy, and G. J. Hannon.** 2002. Stable suppression of gene expression by RNAi in mammalian cells. Proc. Natl. Acad. Sci. USA **99:**1443–1448.
22. **Peunova, N., and G. Enikolopov.** 1995. Nitric oxide triggers a switch to growth arrest during differentiation of neuronal cells. Nature **375:**68–73.
23. **Poyurovsky, M. V., and C. Prives.** 2006. Unleashing the power of p53: lessons from mice and men. Genes Dev. **20:**125–131.
24. **Sharma, R. V., E. Tan, S. Fang, M. V. Gurjar, and R. C. Bhalla.** 1999. NOS gene transfer inhibits expression of cell cycle regulatory molecules in vascular smooth muscle cells. Am. J. Physiol. **276:**H1450–H1459.
25. **Tanner, F. C., P. Meier, H. Greutert, C. Champion, E. G. Nabel, and T. F. Luscher.** 2000. Nitric oxide modulates expression of cell cycle regulatory proteins: a cytostatic strategy for inhibition of human vascular smooth muscle cell proliferation. Circulation **101:**1982–1989.
26. **Zhou, B. B., and S. J. Elledge.** 2000. The DNA damage response: putting checkpoints in perspective. Nature **408:**433–439.